GEOLOGY

E: geology@geosociety.org
W: geosociety.org/gsa
T: @geosociety

# Two-pronged kill mechanism at the end-Triassic mass extinction

**Tracking no:** G49560R

**Authors:**
Calum Fox (WA-OIGC), Jessica Whiteside (University of Southampton), Paul Olsen (Columbia University), Xingqian Cui (University of Florida), Roger Summons (Massachusetts Institute of Technology), Erdem Idiz (Oxford University), and Kliti Grice (Curtin University)

**Abstract:**
High-resolution biomarker and compound-specific isotope distributions, coupled with the degradation of calcareous fossil remnants reveal that intensive euxinia and decalcification (acidification) driven by Central Atlantic Magmatic Province (CAMP) activity formed a two-pronged kill mechanism at the end-Triassic mass extinction. In a newly proposed extinction interval for the basal Blue Lias Formation (Bristol Channel Basin, UK), biomarker distributions reveal an episode of persistent photic zone euxinia (PZE) that extended further upwards into the surface waters. In the same interval shelly taxa almost completely disappear. Beginning in the basal paper shales of the Blue Lias Formation, a Lilliput assemblage consisting of only rare calcitic oysters (Liostrea) and ghost fossils of decalcified aragonitic bivalves are preserved. The stressors of PZE and decalcification parsimoniously explain the extinction event and inform possible combined causes of other biotic crises linked to emplacements of large igneous provinces, notably the end-Permian mass extinction where PZE occurred on a broad and perhaps global scale.

# Two-pronged kill mechanism at the end-Triassic mass extinction

**Calum P. Fox[1 # *], Jessica H. Whiteside[2], Paul E. Olsen[3], Xingqian Cui[4, 5], Roger E. Summons[5], Erdem Idiz[6], Kliti Grice[1]**

*[1]Western Australia Organic Isotope and Geochemistry Centre, School of Earth and Planetary Sciences, The Institute for Geoscience Research, Curtin University, Perth, 6845, Australia*

*[2]Ocean and Earth Science, National Oceanography Centre Southampton, University of Southampton, Southampton, SO14 3ZH, UK*

*[3]Dept. of Earth and Environmental Sciences, Lamont-Doherty Earth Observatory of Columbia University, Palisades, NY 10964, USA*

*[4]School of Oceanography, Shanghai Jiao Tong University, 200030 Shanghai, China*

*[5]Dept. of Earth, Atmospheric and Planetary Sciences, Massachusetts Institute of Technology, MA 02139, USA*

*[6]Dept. of Earth Science, University of Oxford, Oxford, OX1 3AN, UK*

** E-mail: calum.fox@postgrad.curtin.edu.au*

*[#]Now at Dept. of Earth Sciences, Khalifa University, PO Box 127788, Abu Dhabi, UAE*

**ABSTRACT**

High-resolution biomarker and compound-specific isotope distributions, coupled with the degradation of calcareous fossil remnants reveal that intensive euxinia and decalcification (acidification) driven by Central Atlantic Magmatic Province (CAMP) activity formed a two-pronged kill mechanism at the end-Triassic mass extinction. In a newly proposed extinction interval for the basal Blue Lias Formation (Bristol Channel Basin, UK), biomarker distributions reveal an episode of persistent photic zone euxinia (PZE) that extended further upwards into the surface waters. In the same interval shelly taxa almost completely disappear. Beginning in the basal paper shales of the Blue Lias Formation, a Lilliput assemblage consisting of only rare calcitic oysters (*Liostrea*) and ghost fossils of decalcified aragonitic bivalves are preserved. The stressors of PZE and decalcification parsimoniously explain the extinction event and inform possible combined causes of other biotic crises linked to emplacements of large igneous provinces, notably the end-Permian mass extinction where PZE occurred on a broad and perhaps global scale.

## INTRODUCTION

The end-Triassic extinction (ETE; ca. 202 Ma) is one of the largest mass extinction events of the Phanerozoic and temporally correlated with emplacement of the Central Atlantic Magmatic Province (CAMP) (Pálfy et al., 2001). Pulsed CAMP outgassing of $CO_2$ and $SO_2$ in large quantities is thought to have triggered the ETE through a cascading series of environmental perturbations, including global carbon cycle changes, rapid warming leading to 'hyperthermal' climatic events, and increased continental weathering. In many marine sedimentary basins such conditions led to stagnation, deoxygenation, and deposition of organic-rich laminated mudstones (e.g., Kasprak et al., 2015). However, the precise mechanism(s) responsible for the extinction event remain elusive.

The Bristol Channel Basin, SW UK, although not necessarily globally representative, has become a focal locality for ETE studies employing palynological, paleontological (Warrington et al., 2008 and refs therein), and geochemical analyses (Jaraula et al., 2013; Fox et al., 2020). The pronounced negative anomaly in the organic carbon isotope record ($\delta^{13}C_{org}$; initial CIE; Fig. 1) in the Lilstock Formation (Fm.) at St. Audrie's Bay (Hesselbo et al., 2002) is routinely used to chemostratigraphically correlate the extinction event and CAMP volcanism among sections on a global scale (e.g., Hesselbo et al., 2002). However, this CIE is stratigraphically offset from the highest occurrences (HO) of key fossil taxa. For example, the HO of foraminiferal, ostracod, and bivalve fauna (Hallam, 1990) is in the overlying basal Blue Lias Fm. at the base of finely laminated organic carbon-rich mudstones termed the paper shales (Richardson, 1911). Furthermore, the HO of conodonts also sits in the lowermost Blue Lias Fm. (Swift, 1989). Based on these and other findings, including the HO of the reptile clade Phytosauria in the lowermost Blue Lias Fm. (Maisch and Kapitzke, 2010) and a Lilliput assemblage of bivalves at the very

base of the paper shales (Fox et al., 2020), recent studies have placed the ETE above the initial CIE in the paper shales, at a separate and slightly younger $\delta^{13}C_{org}$ anomaly (Fig. 1) (Wignall and Atkinson, 2020; Fox et al., 2020). Despite decades of study establishing the presence of extinction of fauna characteristic of the end-Triassic (Fig. 1) and a dearth of calcite- and aragonite-secreting organisms at the extinction horizon, little is known of the killing mechanism(s). To better investigate this critical interval and the cause(s) of the ETE, we undertook high-resolution (i.e. cm-scale) biomarker and compound-specific isotope analyses to disentangle ecological community shifts recorded in the fossil record at two sections in the Bristol Channel Basin: St. Audrie's Bay [51.182833°, −3.286000°] and Lilstock [51.200757°, −3.176389].

## RESULTS AND DISCUSSION

### Acidification and photic zone euxinia forcing the ETE

Decalcified bivalve taxa exhibiting low diversity (Fox et al., 2020) and a general lack of $CaCO_3$-secreting organisms (Hallam, 1990) above the Lilliput assemblage in the paper shales gives evidence of an acidification event that terminated with the return of calcareous nannoplankton and ammonites later in the sedimentary record (Fig. 1). Termed the biocalcification crisis, this event is placed between the HO of the ammonite *Choristoceras marshi* and lowest occurrence of *Psiloceras spelae* in European sections (McRoberts et al., 2012). Correlation between the HO of conodonts in the SW UK (Swift, 1989) to the HO of Triassic conodonts at the end of the *C. marshi* zone (Hillebrandt et al., 2013) provides correlative evidence of acidification at the ETE. In a global context, the biocalcification crisis is evidenced by major reduction in sedimentary carbonates and biogenic carbonates from secreting organisms,

82 particularly corals, calcareous nannoplankton, benthic foraminifera groups, and some bivalves
83 (Cope and Hallam, 1991; Hautmann, 2004; van de Schootbrugge et al., 2007; Lindström et al.,
84 2012; McRoberts et al., 2012; Fox et al., 2020). Likely driven by CAMP-induced rapid
85 outgassing of $CO_2$, acidification is a plausible kill mechanism. However, our biomarker and
86 compound-specific isotope investigation reveals that additional ecological stresses may play
87 important roles in driving extinction.

88 The paper shales are characterized by low pristane to phytane ratios (Pr/Ph), high
89 gammacerane index values, supporting anoxia in a well-stratified water column, and increases in
90 $C_{40}$ carotenoids derived from purple sulfur bacteria (okenane) and green-pigmented
91 (chlorobactane) and brown-pigmented (isorenieratane) green sulfur bacteria (Fig. 2). Whereas
92 purple sulfur bacteria (Chromatiaceae) and green-pigmented green sulfur bacteria (Chlorobi)
93 reported below this unit indicate the presence of microbial mats (Fox et al., 2020), coexistence
94 with brown-pigmented Chlorobi and biomarkers for anoxia and stratification indicate photic
95 zone euxinia (PZE), a condition in which toxic $H_2S$ extends upward into the sun-lit region of an
96 anoxic water column (e.g. Grice et al., 2005). Due to higher light intensity requirements of
97 Chromatiaceae and green-pigmented Chlorobi compared to brown-pigmented Chlorobi (Grice et
98 al., 1998; Brocks and Schaeffer, 2008; Overmann, 2008), the ratio of isorenieratane to okenane
99 and chlorobactane (iso/oke + chlo) serves as a proxy for the relative depth of the chemocline,
100 where higher values indicate predominance of low-light-adapted photosynthetic bacteria and
101 therefore a deeper chemocline. Thus, the lower paper shales are characterized by a shallower
102 chemocline compared to later in the record where iso/oke + chlo values increase. Below the Blue
103 Lias Fm. iso/oke + chlo values are also low. However, this interval is characterized by

geochemical and sedimentological evidence for shallowing, freshening, and desiccation, but little evidence for prolonged PZE (Fox et al., 2020 and refs therein).

Where okenane and chlorobactane abundances are highest, the $\delta^{13}C_{29}$ *n*-alkane mirrors the minor negative $\delta^{13}C_{org}$ excursion, possibly related to the CAMP (Fig. 3). $\delta^{13}C$ values of regular isoprenoids (pristane and phytane) and *n*-alkanes ($C_{17-19}$) also show negative excursions, albeit more variable (Fig. 3). Significant decreases in okenane and chlorobactane abundances later in the paper shales (Fig. 2) are possibly related to lower-light availability due to a deepening of the chemocline and/or due to increased algal productivity in the euphotic zone (Grice et al., 1998; Brocks and Schaeffer, 2008; Overmann, 2008). Here, $\delta^{13}C$ values of pristane, phytane and $C_{17-19}$ *n*-alkanes show a positive isotope excursion, and based on their isotopic differences, carbon fixation shifts to increased autotrophic production (Fig. 3) (Grice et al., 2005). Elevated isorenieratane abundances in this interval show PZE continued but was limited to the lower region of the photic zone, and low Pr/Ph and aryl isoprenoid ratios throughout the paper shales demonstrate persistent PZE (Fig. 2; Data Repository) (Schwark and Frimmel, 2004).

These results suggest the paper shales formed in two sequential different depositional environments which are related to chemocline depth and carbon isotope chemistry. First, at the extinction horizon in the basal Blue Lias Fm., high abundances of Chromatiaceae and green-pigmented Chlorobi biomarkers and low iso/oke + chlo values support a shallow chemocline with PZE extending throughout much of the photic zone. Biomarker $\delta^{13}C$ values of marine organisms show a negative excursion, are variable compared to isotopic shifts in higher land plants. In modern-day ecosystems, pH changes impact carbon leakage, mechanisms of carbon concentration, and activity of carbonic anhydrase in dehydrating $HCO_3^-$, all of which affect carbon isotope fractionation in phytoplankton (Wang et al., 2016). These effects of acidification

on phytoplankton, in conjunction with intense PZE and its associated precipitation of bio-essential elements (Takahashi et al., 2014), possibly account for the marine $\delta^{13}C$ variations at the extinction horizon. The second depositional environment is characterized by a decline in Chromatiaceae and green-pigmented Chlorobi and increases in brown-pigmented Chlorobi and iso/oke + chlo, consistent with contraction of sulfidic conditions. The coinciding shift to autotrophic production and positive $\delta^{13}C$ excursions in biomarkers of marine organisms agree with a $^{13}C$-enriched euphotic zone due to increased carbon fixation and reduced light availability to Chromatiaceae and Chlorobi. Elevated abundances in brown-pigmented Chlorobi biomarkers support continued PZE but restricted to lower-light levels of the water column.

The invocation of $H_2S$ toxicity as a driver for the ETE is supported by increases in isorenieratane, aryl isoprenoids (Richoz et al., 2012; Jaraula et al., 2013; Kasprak et al., 2015) or pyrite framboid diameter analysis (Atkinson and Wignall, 2019). However, for the first time we report PZE was not only persistent, but due to increased abundances of biomarkers derived from sulfur bacteria that require elevated light intensities and $H_2S$, PZE extended into shallower depths of the photic zone than previously thought. The presence of these organisms supports increased stress to epipelagic nektonic and planktonic communities. Furthermore, increased precipitation of bio-essential elements associated with periods of PZE have suppressive effects on marine life and its recovery during extinction events (Takahashi et al., 2014). Given that PZE biomarkers are observed in European and Canadian sections, which represent a range of depositional settings including open ocean (Richoz et al., 2012; Jaraula et al., 2013; Kasprak et al., 2015), PZE at the ETE may have global extent, although perhaps not everywhere simultaneously. Effects of euxinia on calcifying organisms are poorly understood, but short-term intervals have resulted in planktonic foraminifera extinction (Oba et al., 2011). In conjunction

150 with acidification, PZE may thus explain the near lack of fauna during the ETE biocalcification
151 crisis. Additionally, we note that the importance of anoxia has been shown to be an important
152 stressor on modern coral analogues experimentally (Altieri et al., 2017), and that ocean anoxic
153 events frequently result in a species richness decline in calcareous and benthic communities (e.g.
154 Watkins et al., 2005; Mattioli et al., 2008). Consequently, we argue that the development of
155 persistent and intense PZE in conjunction with acidification leads to major ecological stress, and
156 that these conditions together are important for driving the ETE. These features are the most
157 compelling evidence of CAMP-induced environmental perturbations throughout the latest
158 Rhaetian, and plausibly relate the negative $\delta^{13}C$ anomaly in the lower Blue Lias Fm. to CAMP
159 activity.

160 Organic-rich laminated lithologies are often host to Lagerstätten assemblages that
161 preserve articulated fossils. Lack of bioturbation and preservation of microlaminations in
162 lacustrine and marine settings indicates deposition below the wave base and persistent water
163 column stratification and bottom water anoxia (Olsen, 1990). Although the facies of the paper
164 shales conform to this model, the absence of fish or any articulated fossils (Hallam, 1991;
165 confirmed by our field observations) is consistent with acidification and PZE driving extinction,
166 although this may also be related to basin restriction. This lack of fossil content, in addition to
167 the micro-laminations, is anomalous compared to superficially similar orbitally paced units
168 above the paper shales that do have abundance fossils. From field observations, the paper shales
169 immediately succeeding the Lilliput assemblage are nearly devoid of shelly taxa with the
170 exception of decalcified bivalves, supporting acidification. However, Mander et al., (2008) report
171 shelly taxa specimens (*Modiolus sp.*, *Liostrea sp.*, and *L. hisingeri*) in the upper-most layers, and
172 Atkinson and Wignall (2019) report *Liostrea sp*. in the lower paper shales (Fig. 4) that could be

associated with the lilliput assemblage. Above the paper shales, shelly taxa species richness increases in close proximity to the lowest occurrence of organisms that preserve the aragonitic nacre; *Psiloceras. planorbis* and other *Psiloceras* and *Neophyllites?* ammonites (Warrington et al., 2008 and refs therein). Major increases in foraminifera species richness and preserved foraminiferal test linings occur above this interval (Bonis et al., 2010; Clémence and Hart, 2013), signaling diminishing effects of acidification (Fig. 4). Biomarker and pyrite framboid analysis in shale/dark marl lithologies support cyclical euxinic conditions into the *P. planorbis* zone (Jaraula et al., 2013; Atkinson and Wignall, 2019), suggesting stable conditions with increased continental weathering during shale/dark marl deposition and storm events/mixing during limestone and light marl formation (Weedon et al., 2017). Above the lowest occurrence of *P. planorbis*, bivalve assemblages increase in diversity but not in abundance (Mander et al., 2008) suggesting localized effects of acidification and PZE inhibit the return of pre-extinction ecological conditions.

## CONCLUSIONS

The fully marine expression of the ETE in the SW UK is in the basal Blue Lias Fm., during an acidification event with persistent and intense PZE and its associated redox conditions. This combination of ecological stressors explains many observations within the lower Blue Lias Fm., including the lack of well-preserved vertebrate fossils, near absence of shelly taxa in the paper shales, and subsequent increases in species richness upward toward the termination of the biocalcification crisis. Furthermore, acidic and euxinic conditions constitute the most compelling evidence of CAMP-induced environmental perturbations thought to drive the ETE throughout the latest Rhaetian. In future studies, high-resolution sampling for biomarkers and their $\delta^{13}C$

values, in conjunction with ecological community shifts, will be critical to properly evaluate the global extent and significance of combined ecological stressors in the ETE and similar extinctions.

## ACKNOWLEDGMENTS

**Acknowledgments:** We acknowledge Peter Hopper, Alex Holman, and P. Sargent Bray for technical support. **Funding:** Fox acknowledges Curtin Uni., European Association of Organic Geochemistry, and Khalifa Uni. of Science and Technology (CIRA-2019-066). Fox and Grice thank the ARC (LP150100341; LE110100119; LE100100041; LE0882836). Whiteside and Summons thank the NSF (EAR 1147402). Cui and Summons acknowledge the Simons Foundation Collaboration on the Origins of Life (290361FY18). Olsen acknowledges the Lamont Climate Center. **Competing interests:** Authors declare no competing interests.

## REFERENCES CITED

Altieri, A.H., Harrison, S.B., Seemann, J., Collin, R., Diaz, R.J., and Knowlton, N., 2017, Tropical dead zones and mass mortalities on coral reefs: Proceedings of the National Academy of Sciences, v. 114, p. 3660 LP – 3665, doi:10.1073/pnas.1621517114.

Atkinson, J.W., and Wignall, P.B., 2019, How quick was marine recovery after the end-Triassic mass extinction and what role did anoxia play? Palaeogeography, Palaeoclimatology, Palaeoecology, v. 528, p. 99–119, doi:https://doi.org/10.1016/j.palaeo.2019.05.011.

Bonis, N.R., Ruhl, M., and Kürschner, W.M., 2010, Milankovitch-scale palynological turnover across the Triassic-Jurassic transition at St. Audrie's Bay, SW UK: Journal of the Geological Society, v. 167, p. 877–888, doi:10.1144/0016-76492009-141.

Brocks, J.J., and Schaeffer, P., 2008, Okenane, a biomarker for purple sulfur bacteria (Chromatiaceae), and other new carotenoid derivatives from the 1640Ma Barney Creek Formation: Geochimica et Cosmochimica Acta, v. 72, p. 1396–1414, doi:https://doi.org/10.1016/j.gca.2007.12.006.

Clémence, M.-E., and Hart, M.B., 2013, Proliferation of Oberhauserellidae during the recovery following the Late Triassic extinction: paleoecological implications: Journal of Paleontology, v. 87, p. 1004–1015, doi:DOI: 10.1666/13-021.

Cope, J.C.W., and Hallam, A., 1991, Discussion on correlation of the Triassic–Jurassic boundary in England and Austria: Journal of the Geological Society, v. 148, p. 420–422, doi:10.1144/gsjgs.148.2.0420.

Fox, C.P., Cui, X., Whiteside, J.H., Olsen, P.E., Summons, R.E., and Grice, K., 2020, Molecular and isotopic evidence reveals the end-Triassic carbon isotope excursion is not from massive exogenous light carbon: Proceedings of the National Academy of Sciences, v. 117, p. 30171 LP – 30178, doi:10.1073/pnas.1917661117.

Grice, K., Cao, C., Love, G.D., Böttcher, M.E., Twitchett, R.J., Grosjean, E., Summons, R.E., Turgeon, S.C., Dunning, W., and Jin, Y., 2005, Photic Zone Euxinia During the Permian-Triassic Superanoxic Event: Science, v. 307, p. 706 LP – 709, doi:10.1126/science.1104323.

Grice, K., Schouten, S., Peters, K.E., and Sinninghe Damsté, J.S., 1998, Molecular isotopic characterisation of hydrocarbon biomarkers in Palaeocene–Eocene evaporitic, lacustrine source rocks from the Jianghan Basin, China: Organic Geochemistry, v. 29, p. 1745–1764, doi:https://doi.org/10.1016/S0146-6380(98)00075-8.

Hallam, A., 1990, Correlation of the Triassic-Jurassic boundary in England and Austria: Journal of the Geological Society, v. 147, p. 421–424, doi:10.1144/gsjgs.147.3.0421.

Hautmann, M., 2004, Effect of end-Triassic $CO_2$ maximum on carbonate sedimentation and marine mass extinction: Facies, v. 50, p. 257–261, doi:10.1007/s10347-004-0020-y.

Hesselbo, S.P., Robinson, S.A., Surlyk, F., and Piasecki, S., 2002, Terrestrial and marine

247 extinction at the Triassic-Jurassic boundary synchronized with major carbon-cycle
248 perturbation: A link to initiation of massive volcanism? Geology, v. 30, p. 251–254,
249 https://doi.org/10.1130/0091-7613(2002)030%3C0251:TAMEAT%3E2.0.CO.
250 Hillebrandt, A. V. et al., 2013, The global stratotype sections and point (GSSP) for the base of
251 the jurassic system at kuhjoch (Karwendel Mountains, Northern Calcareous Alps, Tyrol,
252 Austria): Episodes, v. 36, p. 162–198, doi:10.18814/epiiugs/2013/v36i3/001.
253 Jaraula, C.M.B., Grice, K., Twitchett, R.J., Böttcher, M.E., LeMetayer, P., Dastidar, A.G., and
254 Opazo, L.F., 2013, Elevated $pCO_2$ leading to Late Triassic extinction, persistent photic zone
255 euxinia, and rising sea levels: Geology, v. 41, p. 955–958, doi:10.1130/G34183.1.
256 Kasprak, A.H., Sepúlveda, J., Price-Waldman, R., Williford, K.H., Schoepfer, S.D., Haggart,
257 J.W., Ward, P.D., Summons, R.E., and Whiteside, J.H., 2015, Episodic photic zone euxinia
258 in the northeastern Panthalassic Ocean during the end-Triassic extinction: Geology, v. 43, p.
259 307–310, doi:10.1130/G36371.1.
260 Lindström, S., van de Schootbrugge, B., Dybkjær, K., Pedersen, G.K., Fiebig, J., Nielsen, L.H.,
261 and Richoz, S., 2012, No causal link between terrestrial ecosystem change and methane
262 release during the end-Triassic mass extinction: Geology, v. 40, p. 531–534,
263 doi:10.1130/G32928.1.
264 Maisch, M.W., and Kapitzke, M., 2010, A presumably marine phytosaur (Reptilia: Archosauria)
265 from the pre-planorbis beds (Hettangian) of England: Neues Jahrbuch für Geologie und
266 Paläontologie - Abhandlungen, v. 257, p. 373–379, doi:10.1127/0077-7749/2010/0076.
267 Mander, L., Twitchett, R.J., and Benton, M.J., 2008, Palaeoecology of the Late Triassic
268 extinction event in the SW UK: Journal of the Geological Society, v. 165, p. 319–332,
269 doi:10.1144/0016-76492007-029.

Mattioli, E., Pittet, B., Suan, G., and Mailliot, S., 2008, Calcareous nannoplankton changes across the early Toarcian oceanic anoxic event in the western Tethys: Paleoceanography, v. 23, doi:https://doi.org/10.1029/2007PA001435.

McRoberts, C.A., Krystyn, L., and Hautmann, M., 2012, Macrofaunal response to the end-Triasic mass extinction in the west-Tethyan Kössen Basin, Austria: Paliaos, v. 27, p. 608–617, http://www.jstor.org/stable/23362119.

Oba, M., Kaiho, K., Okabe, T., Lamolda, M.A., and Wright, J.D., 2011, Short-term euxinia coinciding with rotaliporid extinctions during the Cenomanian-Turonian transition in the middle-neritic eastern North Atlantic inferred from organic compounds: Geology, v. 39, p. 519–522, doi:10.1130/G31805.1.

Olsen, P.E., 1990, Tectonic, Climatic, and Biotic Modulation of Lacustrine Ecosystems—Examples from Newark Supergroup of Eastern North America (B. J. Katz, Ed.): Lacustrine Basin Exploration: Case Studies and Modern Analogs, v. 50, p. 0, doi:10.1306/M50523C13.

Overmann, J., 2008, Ecology of Phototrophic Sulfur Bacteria, *in* Hell, R., Dahl, C., Knaff, D., and Leustek, T. eds., Sulfur Metabolism in Phototrophic Organisms, Dordrecht, Springer Netherlands, p. 375–396, doi:10.1007/978-1-4020-6863-8_19.

Pálfy, J., Demény, A., Haas, J., Hetényi, M., Orchard, M.J., and Veto, I., 2001, Carbon isotope anomaly and other geochemical changes at the Triassic-Jurassic boundary from a marine section in Hungary: Geology, v. 29, p. 1047–1050, doi:10.1130/0091-7613(2001)029<1047:CIAAOG>2.0.CO;2.

Richardson, L., 1911, The Rhætic and Contiguous Deposits of West, MID, & Part of East Somerset: Quarterly Journal of the Geological Society, v. 67, p. 1–74, doi:10.1144/GSL.JGS.1911.067.01-04.03.

Richoz, S. et al., 2012, Hydrogen sulphide poisoning of shallow seas following the end-Triassic extinction: Nature Geoscience, v. 5, p. 662–667, doi:10.1038/ngeo1539.

van de Schootbrugge, B., Tremolada, F., Rosenthal, Y., Bailey, T.R., Feist-Burkhardt, S., Brinkhuis, H., Pross, J., Kent, D. V., and Falkowski, P.G., 2007, End-Triassic calcification crisis and blooms of organic-walled “disaster species”: Palaeogeography, Palaeoclimatology, Palaeoecology, v. 244, p. 126–141, doi:10.1016/j.palaeo.2006.06.026.

Schwark, L., and Frimmel, A., 2004, Chemostratigraphy of the Posidonia Black Shale, SW-Germany: II. Assessment of extent and persistence of photic-zone anoxia using aryl isoprenoid distributions: Chemical Geology, v. 206, p. 231–248, doi:https://doi.org/10.1016/j.chemgeo.2003.12.008.

Swift, A., 1989, First records of conodonts from the late Triassic of Britain: Palaeontology, v. 32, p. 325–333.

Takahashi, S., Yamasaki, S., Ogawa, Y., Kimura, K., Kaiho, K., Yoshida, T., and Tsuchiya, N., 2014, Bioessential element-depleted ocean following the euxinic maximum of the end-Permian mass extinction: Earth and Planetary Science Letters, v. 393, p. 94–104, doi:https://doi.org/10.1016/j.epsl.2014.02.041.

Wang, S., Yeager, K.M., and Lu, W., 2016, Carbon isotope fractionation in phytoplankton as a potential proxy for pH rather than for [CO2(aq)]: Observations from a carbonate lake: Limnology and Oceanography, v. 61, p. 1259–1270, doi:https://doi.org/10.1002/lno.10289.

Warrington, G., Cope, J.C.W., and Ivimey-Cook, H.C., 2008, The St Audrie’s Bay-Doniford Bay section, Somerset, England: updated proposal for a candidate Global Stratotype Section and Point for the base of the Hettangian Stage, and of the Jurassic System: International Subcommission on Jurassic Stratigraphy Newsletter, v. 35, p. 2–66.

316 Watkins, D.K., Cooper, M.J., and Wilson, P.A., 2005, Calcareous nannoplankton response to late
317 Albian oceanic anoxic event 1d in the western North Atlantic: Paleoceanography, v. 20,
318 doi:https://doi.org/10.1029/2004PA001097.
319 Weedon, G.P., Jenkyns, H.C., and Page, K.N., 2017, Combined sea-level and climate controls on
320 limestone formation, hiatuses and ammonite preservation in the Blue Lias Formation, South
321 Britain (uppermost Triassic – Lower Jurassic): Geological Magazine, v. 155, p. 1117–1149,
322 doi:DOI: 10.1017/S001675681600128X.
323 Wignall, P.B., and Atkinson, J.W., 2020, A two-phase end-Triassic mass extinction: Earth-
324 Science Reviews, v. 208, p. 103282, doi:10.1016/j.earscirev.2020.103282.
325
326

## FIGURE CAPTIONS

**Figure 1.** $\delta^{13}$Corg records in the SW UK. ETE lithology and paleogeographic reconstruction (top) after Hesselbo et al., (2002), with CAMP lateral extent in red. HO of conodonts after Swift (1989). References for other ecological and geophysical data in figure.

**Figure 2.** Biomarker-inferred redox and PZE conditions at St. Audrie's Bay (circles, solid lines) and Lilstock (squares, dashed lined) relative to $\delta^{13}C_{org}$ and TOC. Two depositional environments indicated by green (shallow redoxcline) and pink (deeper chemocline) bars. Biomarkers below and ecological indicators above each profile. Pristane to phytane ratios and gammacerane, okenane, chlorobactane and isorenieratane indices up to the base of the Blue Lias Fm. reported in Fox et al., (2020). Details in the Data Repository.

**Figure 3.** Compound-specific carbon isotope analysis at St. Audrie's Bay (circles, solid lines) and Lilstock (squares, dashed lines). Two depositional environments indicated by green (variable but negative excursions in regular isoprenoids and *n*-alkanes) and pink (positive excursions and shift to more autotrophy) bars. Biomarkers below, and ecological indicators above each profile. $\delta^{13}$C of biomarkers to the base of the Blue Lias Fm reported in Fox et al., (2020). Details in the Data Repository.

**Figure 4.** Ecological shifts relative to anoxia (paper shales), biocalcification crisis, and PZE in the Bristol Channel Basin. Note bivalve species richness increases after intense PZE and foraminifera species richness increase with return of *P. planorbis*. Details in Data Repository.

# Figure 1

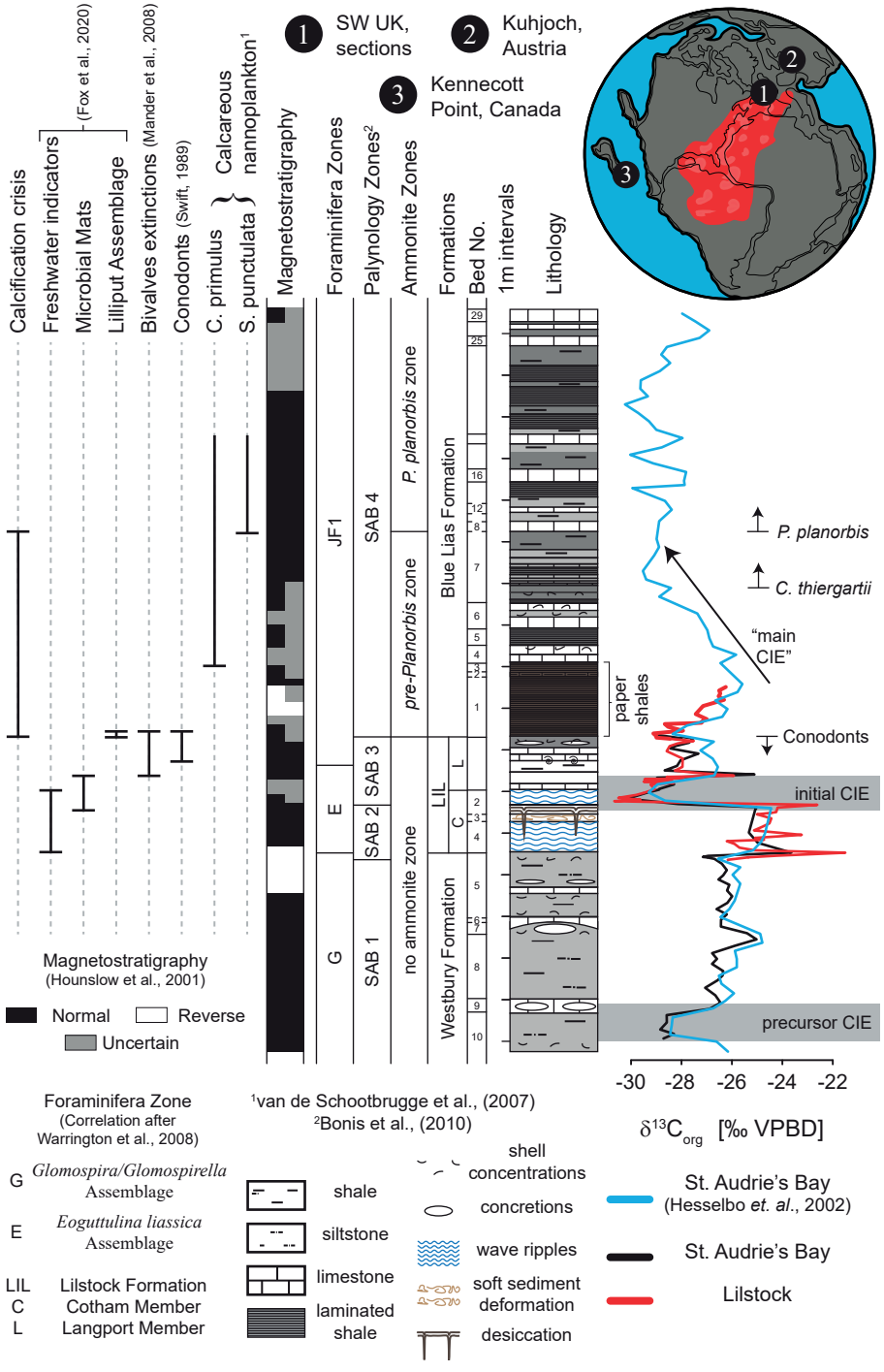
1 SW UK, sections
2 Kuhjoch, Austria
3 Kennecott Point, Canada
Calcification crisis
Freshwater indicators
Microbial Mats
(Fox et al., 2020)
Lilliput Assemblage
Bivalves extinctions (Mander et al., 2008)
Conodonts (Swift, 1989)
C. primulus
Calcareous nannoplankton[1]
S. punctulata
Magnetostratigraphy
Foraminifera Zones
Palynology Zones[2]
Ammonite Zones
Formations
Bed No.
1m intervals
Lithology
JF1
G
E
SAB 1
SAB 2
SAB 3
SAB 4
no ammonite zone
pre-Planorbis zone
P. planorbis zone
Westbury Formation
LIL
C
L
Blue Lias Formation
paper shales
P. planorbis
C. thiergartii
"main CIE"
Conodonts
initial CIE
precursor CIE
-30 -28 -26 -24 -22
δ13Corg [‰ VPBD]
Magnetostratigraphy
(Hounslow et al., 2001)
Normal
Reverse
Uncertain
Foraminifera Zone
(Correlation after Warrington et al., 2008)
G Glomospira/Glomospirella Assemblage
E Eoguttulina liassica Assemblage
LIL Lilstock Formation
C Cotham Member
L Langport Member
[1]van de Schootbrugge et al., (2007)
[2]Bonis et al., (2010)
shale
siltstone
limestone
laminated shale
shell concentrations
concretions
wave ripples
soft sediment deformation
desiccation
St. Audrie's Bay (Hesselbo et. al., 2002)
St. Audrie's Bay
Lilstock

# Figure 2

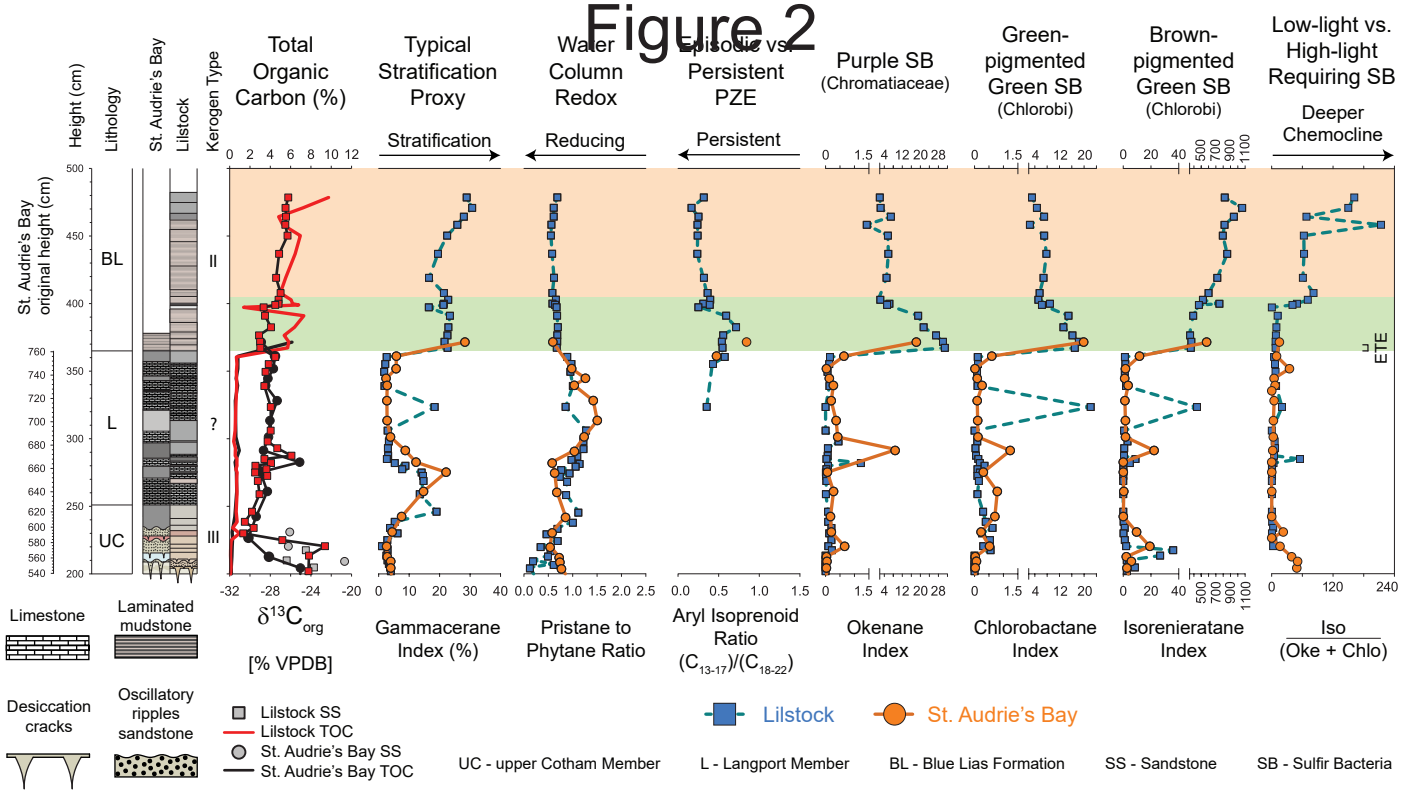
Height (cm)
Lithology
St. Audrie's Bay Lilstock
Kerogen Type
Total Organic Carbon (%)
Typical Stratification Proxy
Water Column Redox
Episodic vs. Persistent PZE
Purple SB (Chromatiaceae)
Green-pigmented Green SB (Chlorobi)
Brown-pigmented Green SB (Chlorobi)
Low-light vs. High-light Requiring SB
Deeper Chemocline
Stratification
Reducing
Persistent
St. Audrie's Bay original height (cm)
BL
L
UC
II
?
III
ETE
δ13Corg [% VPDB]
Gammacerane Index (%)
Pristane to Phytane Ratio
Aryl Isoprenoid Ratio (C13-17)/(C18-22)
Okenane Index
Chlorobactane Index
Isorenieratane Index
Iso / (Oke + Chlo)
Limestone
Laminated mudstone
Desiccation cracks
Oscillatory ripples sandstone
Lilstock SS
Lilstock TOC
St. Audrie's Bay SS
St. Audrie's Bay TOC
Lilstock
St. Audrie's Bay
UC - upper Cotham Member
L - Langport Member
BL - Blue Lias Formation
SS - Sandstone
SB - Sulfir Bacteria

# Figure 3

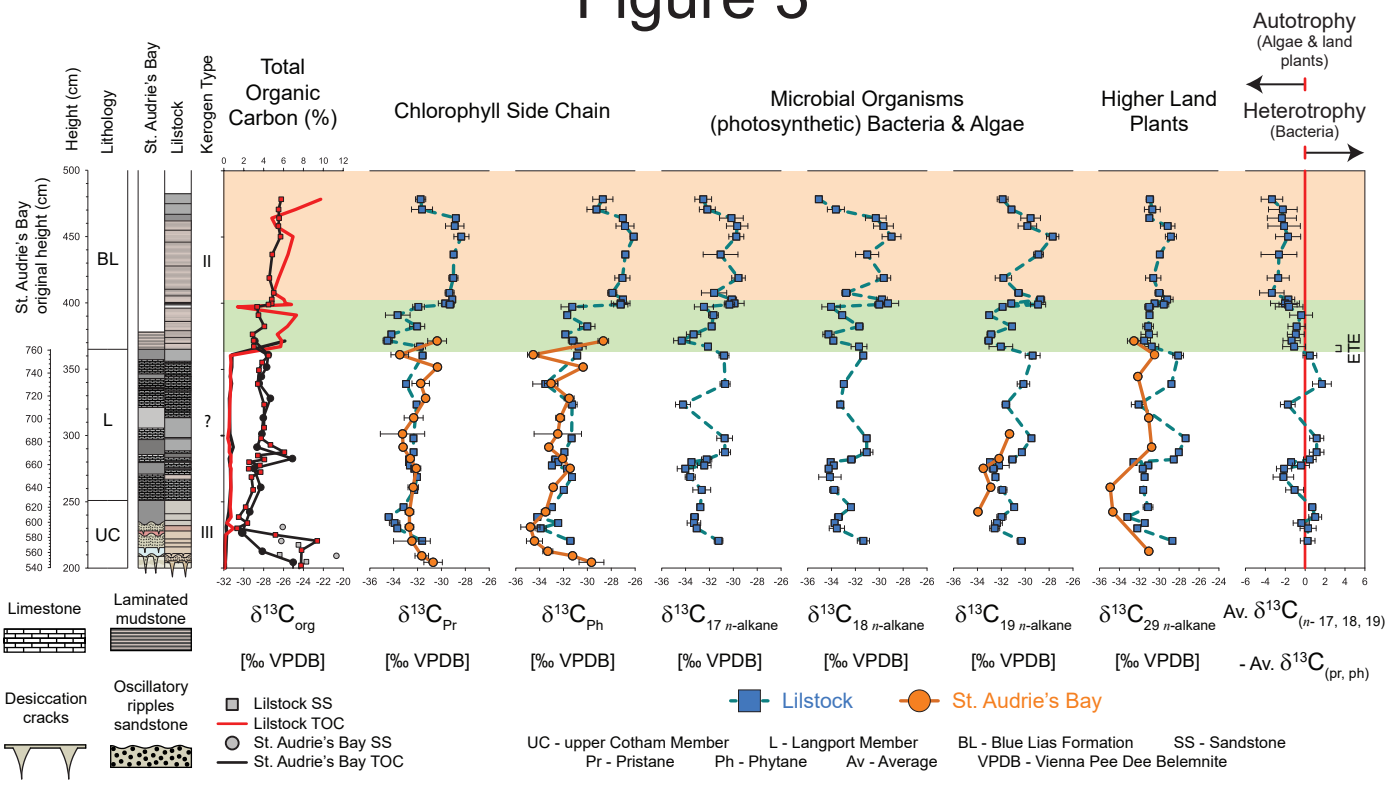
Autotrophy
(Algae & land plants)
Heterotrophy
(Bacteria)
Height (cm)
Lithology
St. Audrie's Bay Lilstock
Kerogen Type
Total Organic Carbon (%)
Chlorophyll Side Chain
Microbial Organisms (photosynthetic) Bacteria & Algae
Higher Land Plants
St. Audrie's Bay original height (cm)
BL
L
UC
II
?
III
ETE
Limestone
Laminated mudstone
Desiccation cracks
Oscillatory ripples sandstone
Lilstock SS
Lilstock TOC
St. Audrie's Bay SS
St. Audrie's Bay TOC
δ13Corg [‰ VPDB]
δ13CPr [‰ VPDB]
δ13CPh [‰ VPDB]
δ13C17 n-alkane [‰ VPDB]
δ13C18 n-alkane [‰ VPDB]
δ13C19 n-alkane [‰ VPDB]
δ13C29 n-alkane [‰ VPDB]
Av. δ13C(n- 17, 18, 19) - Av. δ13C(pr, ph)
Lilstock
St. Audrie's Bay
UC - upper Cotham Member
L - Langport Member
BL - Blue Lias Formation
SS - Sandstone
Pr - Pristane
Ph - Phytane
Av - Average
VPDB - Vienna Pee Dee Belemnite

# Figure 4

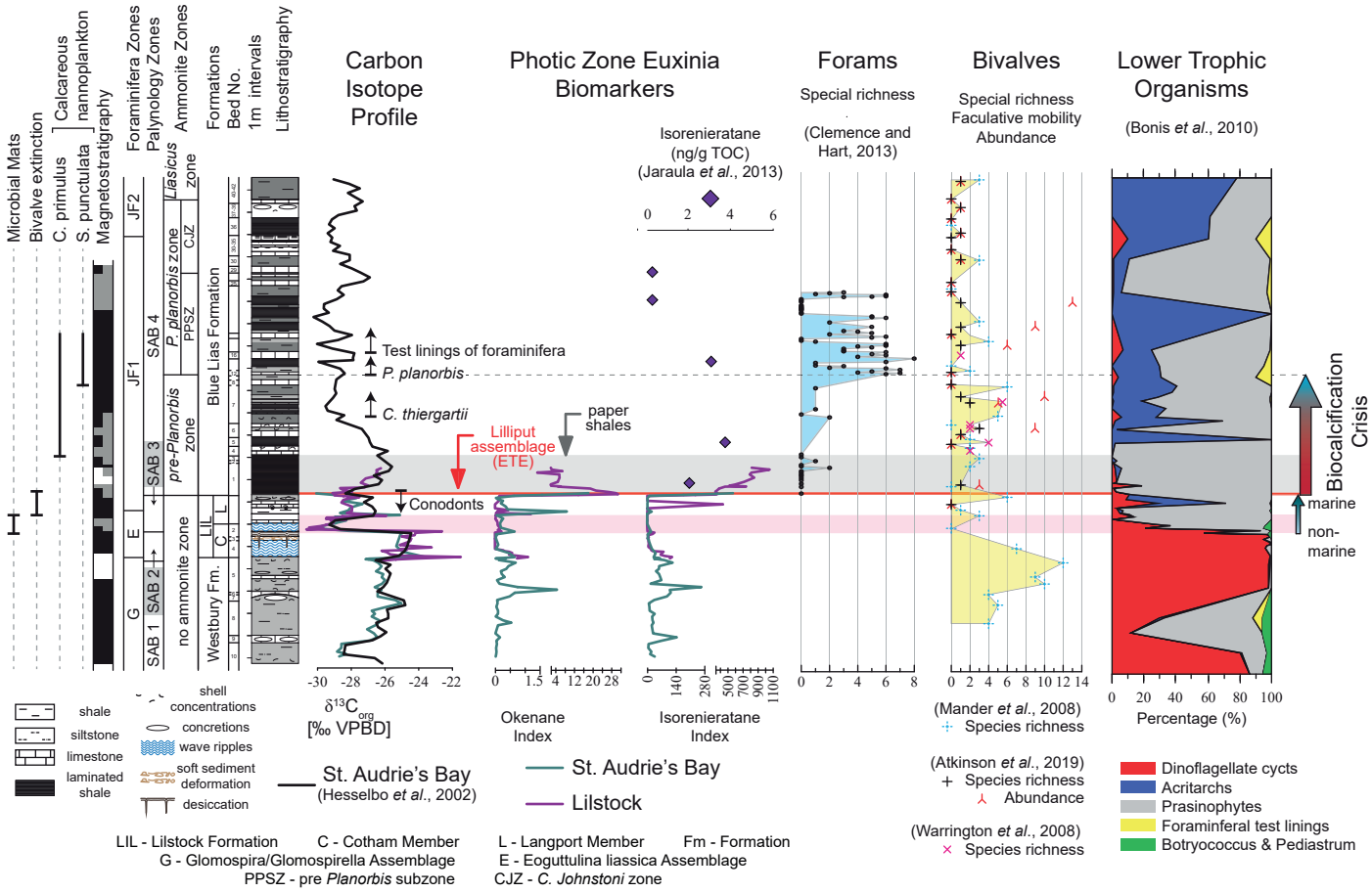
Microbial Mats
Bivalve extinction
C. primulus
S. punctulata
Magnetostratigraphy
Calcareous nannoplankton
Foraminifera Zones
Palynology Zones
Ammonite Zones
Formations
Bed No.
1m intervals
Lithostratigraphy
JF2
JF1
G
E
SAB 4
SAB 3
SAB 2
SAB 1
Liasicus zone
P. planorbis zone
C.JZ
PPSZ
pre-Planorbis zone
no ammonite zone
Blue Lias Formation
LIL
C
L
Westbury Fm.
Carbon Isotope Profile
Photic Zone Euxinia Biomarkers
Forams
Bivalves
Lower Trophic Organisms
Isorenieratane (ng/g TOC) (Jaraula et al., 2013)
Special richness
(Clemence and Hart, 2013)
Special richness
Faculative mobility
Abundance
(Bonis et al., 2010)
Test linings of foraminifera
P. planorbis
C. thiergartii
Lilliput assemblage (ETE)
paper shales
Conodonts
Biocalcification Crisis
marine
non-marine
-30 -28 -26 -24 -22
δ13Corg [‰ VPBD]
St. Audrie's Bay (Hesselbo et al., 2002)
0 1.5 4 12 20 28
Okenane Index
0 140 280 500 700 900 1100
Isorenieratane Index
St. Audrie's Bay
Lilstock
0 2 4 6 8
0 2 4 6 8 10 12 14
(Mander et al., 2008)
Species richness
(Atkinson et al., 2019)
Species richness
Abundance
(Warrington et al., 2008)
Species richness
0 20 40 60 80 100
Percentage (%)
Dinoflagellate cycts
Acritarchs
Prasinophytes
Foraminferal test linings
Botryococcus & Pediastrum
shale
siltstone
limestone
laminated shale
shell concentrations
concretions
wave ripples
soft sediment deformation
desiccation
LIL - Lilstock Formation
C - Cotham Member
G - Glomospira/Glomospirella Assemblage
PPSZ - pre Planorbis subzone
L - Langport Member
Fm - Formation
E - Eoguttulina liassica Assemblage
CJZ - C. Johnstoni zone